



1 Measurement report: Size-resolved mass concentration of equivalent 2 black carbon-containing particle larger than 700 nm and its role in 3 radiation

4 Weilun Zhao¹, Ying Li^{2,3}, Gang Zhao⁴, Song Guo⁴, Nan Ma⁵, Shuya Hu⁴, Chunsheng Zhao¹

5 ¹Department of Atmospheric and Oceanic Sciences, School of Physics, Peking University, Beijing 100871, China

6 ²Department of Ocean Science and Engineering, Southern University of Science and Technology, Shenzhen 518055, China

7 ³Southern Marine Science and Engineering Guangdong Laboratory, Guangzhou 511458, China

8 ⁴State Key Joint Laboratory of Environmental Simulation and Pollution Control, College of Environmental Sciences and
9 Engineering, Peking University, Beijing 100871, China

10 ⁵Institute for Environmental and Climate Research, Jinan University, Guangzhou 511443, China

11 Correspondence to: Chunsheng Zhao (zcs@pku.edu.cn)

12 **Abstract.** Black carbon (BC) mass size distribution (BCMSD) is crucial in both environment and climate system due to BC's
13 intense size-dependent absorption of solar radiation. BC-containing particles of size larger than 700 nm ($BC_{>700}$) could
14 contribute to larger than half of bulk BC mass concentration. Unfortunately, previous methods concentrated on BC-containing
15 particles less than 700 nm because of technical limitation. The contribution of BC to absorption and radiative effect would be
16 underestimated without consideration of $BC_{>700}$. In this study, equivalent BCMSD (eBCMSD) from 150 nm up to 1.5 μm was
17 measured at high time resolution of 1 h for the first time by an aerodynamic aerosol classifier in tandem with an aethalometer
18 in two field campaigns over eastern China, namely Changzhou located in the Yangtze River Delta and Beijing located in the
19 North China Plain. The results revealed that the level of eBCMSD in both Changzhou and Beijing increased with increasing
20 pollution. The pattern of eBCMSD in Changzhou (Beijing) was mostly bimodal (unimodal) peaking at 240 and 1249 nm (427
21 nm). The peak diameter of eBCMSD in Changzhou did not shift significantly with increasing pollution (240 to 289 nm). In
22 contrast, the peak diameter of eBCMSD in Beijing shifted towards larger size from 347 to 527 nm with increasing pollution,
23 indicating the aging process in urban site was different from that in regional background site. eBCMSD in both Changzhou
24 and Beijing had significant diurnal cycle with lower (higher) level of eBCMSD during daytime (nighttime). Equivalent $BC_{>700}$
25 ($eBC_{>700}$) was ubiquitous and varied significantly with different locations and pollution levels. The campaign-averaged
26 contribution of $eBC_{>700}$ to bulk eBC mass concentration ($m_{eBC,bulk}$), bulk absorption coefficient ($\sigma_{ab,bulk}$) as well as estimated
27 direct radiative forcing of eBC (DRF_{eBC}) in Changzhou and Beijing were 27.8 (20.9 ~ 36.5) % and 24.1 (17.5 ~ 34.2) %, 19.6
28 (15.8 ~ 24.6) % and 25.9 (19.6 ~ 33.7) %, as well as 20.5 (18.4 ~ 22.2) % and 21.0 (16.3 ~ 26.1) %, respectively. $m_{eBC,bulk}$,
29 $\sigma_{ab,bulk}$ as well as DRF_{eBC} of $eBC_{>700}$ in Changzhou (Beijing) varied by 3.6 (5.1) times from 0.11 (0.07) to 0.40 (0.36) $\mu\text{g m}^{-3}$,
30 3.2 (5.5) times from 0.54 (0.63) to 1.75 (3.45) Mm^{-1} as well as 2.4 (4.7) times from 0.1 (0.1) to 0.24 (0.47) W m^{-2} , respectively,
31 with the aggravation of pollution. The contribution of $eBC_{>700}$ to $m_{eBC,bulk}$ and $\sigma_{ab,bulk}$ had significant diurnal cycle with higher



32 (lower) fraction during daytime (nighttime) in both Changzhou and Beijing. A case study indicated that the contribution of
33 $e_{BC>700}$ to $m_{eBC,bulk}$, $\alpha_{ab,bulk}$ and DRF_{eBC} could reach up to 50 %, 50 % and 40 %, respectively. It was highly recommended to
34 consider whole size range of BC-containing particles in the model estimation of BC radiative effect.

35 **1 Introduction**

36 Black carbon (BC) is strong light-absorbing carbonaceous particle (Bond and Bergstrom, 2006) from incomplete
37 combustion of fossil fuel or biomass (Bond et al., 2004). Absorption of BC increases light extinction (Moosmuller et al., 2009)
38 and has warming effect on the climate system (Bond, 2001). BC radiative effect had considerable uncertainties and different
39 estimated BC radiative effects did not even converge to same order of magnitude (Bond et al., 2013; Szopa et al., 2021).

40 Previous estimation of BC radiative effect was based on bulk BC mass concentration ($m_{BC,bulk}$) from emission inventory
41 and prescribed mass absorption cross section (MAC) (Bond et al., 2013). Both $m_{BC,bulk}$ and MAC was influenced by BC mass
42 size distribution (BCMSD). BCMSD was one of the BC microphysical properties that BC radiative effect was highly sensitive
43 to (Matsui et al., 2018), and could result in obvious variation in aerosol radiative forcing (Zhao et al., 2019). BCMSD
44 depended on the emission source essentially. For example, the peak diameter of freshly emitted BCMSD from fossil fuel was
45 generally smaller than that from biomass burning (Berner et al., 1984; Artaxo et al., 1998; Schwarz et al., 2008). After BC was
46 emitted to the ambient environment, BCMSD was influenced by BC aging process, during which BC optical properties
47 underwent remarkable changes (Zhang et al., 2008). For instance, BC could be coated by other non-BC materials during
48 atmospheric transport. The existence of non-BC coating enhanced BC absorption and the phenomenon was termed as “lensing
49 effect” (Fuller et al., 1999), of which the accurate quantification was a critical challenge in estimating BC radiative effect (Liu
50 et al., 2017). The information of BCMSD was required to resolve the influence of “lensing effect” on BC radiative forcing.

51 Guo (2016) reported that reported that elemental carbon (EC, Petzold et al. (2013)) containing particles larger than 2.1 μm
52 accounted for 27.6 ~ 35.2 % of bulk EC mass concentration ($m_{EC,bulk}$). Wang et al. (2017) reported that EC-containing particle
53 larger than 1.1 μm accounted for 40.6 ~ 65.5 % of $m_{EC,bulk}$. Wang et al. (2022) indicated that EC-containing particle larger
54 than 1 μm contributed to 50 ~ 54 % of $m_{EC,bulk}$. Therefore, BC-containing particle larger than 1 μm contributed to significant
55 part of total BC mass. Wang et al. (2022) found that these super large carbon-containing particles were super-aggregated BC
56 particles with fractal structure or BC-containing particles with massive coating from secondary processes. It should be noted
57 that current characterization of BC-containing particle larger than 1 μm could be only achieved through EC mass size
58 distribution (ECMSD) measurement by off-line thermo/optical organic carbon/elemental carbon analysis of size-segregated
59 filter-based samples (Chow et al., 2001). The resulting time-resolution of ECMSD was 24 ~ 48 h. Considering that the typical
60 time scale of BC aging was 4 ~ 18 h (Peng et al., 2016), current measured ECMSD could not resolve atmospheric aging of
61 BC-containing particles larger than 1 μm . Actually, current method capable of measuring BC-containing particle on time scale
62 of BC aging, namely laser-induced incandescence technique (Schwarz et al., 2006), was limited to size less than 700 nm. The
63 characterization of BC-containing particles larger than 700 nm ($BC_{>700}$) during atmospheric aging was still unclear. The



64 contribution of $BC_{>700}$ to absorption and BC radiative forcing was lack of study.

65 In this study, equivalent BC (eBC, Petzold et al. (2013)) mass size distribution (eBCMSD) up to $1.5 \mu\text{m}$ was measured with
66 a time resolution of 1 h to study the evolution of equivalent $BC_{>700}$ (eBC $_{>700}$) as well as the contribution of eBC $_{>700}$ to bulk
67 eBC mass concentration ($m_{\text{eBC,bulk}}$), bulk absorption coefficient ($\sigma_{\text{ab,bulk}}$) and eBC direct radiative forcing. eBCMSD was
68 determined by an aerosol aerodynamic classifier (AAC, Cambustion, UK, Tavakoli and Olfert (2013)) in tandem with an
69 aethalometer (model AE33, Magee, USA, Drinovec et al. (2015), AAC – AE33) based on the method proposed by Zhao et al.
70 (2022). eBCMSD was measured in two different locations of eastern China to study the spatial difference of eBC $_{>700}$. Direct
71 radiative forcing of eBC (DRF $_{\text{eBC}}$) was estimated by the Santa Barbara DISORT (discrete ordinates radiative transfer)
72 Atmospheric Radiative Transfer (SBDART) model (Ricchiazzi et al., 1998).

73 The structure of this study was organized as follows. Section 2 introduced the field measurement, instrumental setup, and
74 details about estimation of DRF $_{\text{eBC}}$. Section 3 discussed the evolution as well as mass, absorption and radiation contribution
75 of eBC $_{>700}$ based on the field measurement. Section 4 came to the conclusions.

76 **2 Methods**

77 **2.1 Field measurement**

78 The AAC-AE33 system was first applied to a field measurement in Changzhou, Jiangsu Province, China ($119^{\circ}36'E$, $31^{\circ}43'$
79 N), situated at the Yangtze River Delta, from May 17th to June 3rd in 2021. Then, the AAC-AE33 was deployed in Beijing,
80 China ($116^{\circ}18'E$, $39^{\circ}59'N$), located in the North China Plain, from October 29th 2021 to January 25th 2022. The measurement
81 station in Changzhou was a typical regional background site and the other in Beijing was representative of urban environment.
82 The detailed description of Changzhou and Beijing could be found in Zhao et al. (2022) and Zhao et al. (2019), respectively.

83 **2.2 Instrumental setup**

84 The instrumental setup for eBCMSD measurement was illustrated in detail by Zhao et al. (2022) and introduced here briefly.
85 As shown in Fig. 1, a PM $_{10}$ inlet (16.67 L min^{-1}) was used to sample ambient aerosol particles. Then particles passed through
86 a silica gel diffusion drier, where relative humidity (RH) was decreased to less than 30 %, before sampled by the AAC-AE33.
87 AAC-AE33 measured size-resolved absorption coefficient ($\sigma_{\text{ab,size-resolved}}$) at a flow rate of 3 L min^{-1} in Changzhou and 2 L
88 min^{-1} in Beijing, respectively. AAC was set to scan 12 logarithmically equally distributed aerodynamic sizes ranging from
89 200 nm to $1.5 \mu\text{m}$ in Changzhou and 150 nm to $1.5 \mu\text{m}$ in Beijing, respectively. It should be pointed out that particle diameter
90 (D_p) was aerodynamic size in this study. Particles of each scanned size were sampled for 5 min, so the time resolution of
91 $\sigma_{\text{ab,size-resolved}}$ came to 1 h. The measured $\sigma_{\text{ab,size-resolved}}$ at wavelength of 880 nm by AE33 was used to derive eBCMSD because
92 BC was the major contributor of aerosol absorption at 880 nm (Ramachandran and Rajesh, 2007).

93 MAC was required to convert absorption coefficient to eBC mass concentration. The size-dependent MAC was modeled
94 based on the scheme proposed by Zhao et al. (2021), which required size-resolved particle number concentration ($N_{\text{size-resolved}}$).
95 $N_{\text{size-resolved}}$ was measured by a scanning mobility particle sizer (SMPS, TSI, USA) at 0.3 L min^{-1} as well as an aerodynamic



96 particle sizer (APS, TSI, USA) at 5 L min⁻¹ in Changzhou and an AAC in tandem with condensation particle counter (CPC,
97 TSI, USA, AAC – CPC, Johnson et al. (2018)) at 1 L min⁻¹ in Beijing, respectively. AAC-AE33 measured $\sigma_{ab,size-resolved}$ and
98 determined eBCMSD synchronously. Therefore, the contribution of eBC_{>700} to both bulk absorption and $m_{eBC,bulk}$ could be
99 quantified simultaneously.

100 In this study, the bulk mass concentration of eBC-containing particle ($m_{eBC,bulk}$) was defined as

$$101 \quad m_{eBC,bulk} = \int_{200 \text{ nm}}^{1500 \text{ nm}} \frac{dm_{eBC}}{d \log D_p} d \log D_p, \quad (1)$$

102 where $\frac{dm_{eBC}}{d \log D_p}$ was eBCMSD, and the lower limit of integral was 200 nm in both Changzhou and Beijing for the convenience
103 of comparison. The difference of 50 nm in D_{p0} had little influence the conclusion of this study. The bulk mass concentration
104 of eBC_{>700} ($m_{eBC,bulk,>700}$) was defined as

$$105 \quad m_{eBC,bulk,>700} = \int_{700 \text{ nm}}^{1500 \text{ nm}} \frac{dm_{eBC}}{d \log D_p} d \log D_p. \quad (2)$$

106 The contribution of eBC_{>700} to $m_{eBC,bulk}$ ($f_{m,>700}$) was defined as

$$107 \quad f_{m,>700} = \frac{m_{eBC,bulk,>700}}{m_{eBC,bulk}} \times 100 \%. \quad (3)$$

108 Similarly, the bulk absorption coefficient ($\sigma_{ab,bulk}$) was defined as

$$109 \quad \sigma_{ab,bulk} = \int_{200 \text{ nm}}^{1500 \text{ nm}} \frac{d\sigma_{ab}}{d \log D_p} d \log D_p, \quad (4)$$

110 where $\frac{d\sigma_{ab}}{d \log D_p}$ was $\sigma_{ab,size-resolved}$. The bulk absorption coefficient of eBC_{>700} ($\sigma_{ab,bulk,>700}$) was defined as

$$111 \quad \sigma_{ab,bulk,>700} = \int_{700 \text{ nm}}^{1500 \text{ nm}} \frac{d\sigma_{ab}}{d \log D_p} d \log D_p. \quad (5)$$

112 The contribution of eBC_{>700} to $\sigma_{ab,bulk}$ ($f_{ab,>700}$) was defined as

$$113 \quad f_{ab,>700} = \frac{\sigma_{ab,bulk,>700}}{\sigma_{ab,bulk}} \times 100 \%. \quad (6)$$

114 2.3 Estimation of direct radiative forcing of equivalent black carbon

115 The direct radiative effect was one of the BC characteristics that arouse extensive concerns. The SBDART model was
116 employed to study the characteristics of DRF_{eBC}. Specifically, the instantaneous DRF_{eBC} was estimated at the top of
117 atmosphere (TOA) under the cloud-free condition. Wavelengths from 250 nm to 4 μm were simulated in this study. Direct
118 radiative forcing of aerosol (DRF_{aerosol}) was defined as (Zhao et al., 2018):

$$119 \quad DRF_{aerosol} = (F_{aerosol,\downarrow} - F_{aerosol,\uparrow}) - (F_{clearsky,\downarrow} - F_{clearsky,\uparrow}), \quad (7)$$

120 where $F_{aerosol,\downarrow}$ ($F_{aerosol,\uparrow}$) was downward (upward) radiative irradiance flux at TOA with aerosol, and $F_{clearsky,\downarrow}$
121 ($F_{clearsky,\uparrow}$) was downward (upward) radiative irradiance flux at TOA without aerosol. Direct radiative forcing of aerosol
122 without eBC (DRF_{aerosol,noneBC}) was defined as:

$$123 \quad DRF_{aerosol,noneBC} = (F_{aerosol,noneBC,\downarrow} - F_{aerosol,noneBC,\uparrow}) - (F_{clearsky,\downarrow} - F_{clearsky,\uparrow}), \quad (8)$$

124 where $F_{aerosol,noneBC,\downarrow}$ ($F_{aerosol,noneBC,\uparrow}$) was downward (upward) radiative irradiance flux at TOA with aerosol except eBC.



125 The DRF_{eBC} was defined as the difference between $DRF_{aerosol}$ and $DRF_{aerosol,noneBC}$:

$$126 DRF_{eBC} = (F_{aerosol,\downarrow} - F_{aerosol,\uparrow}) - (F_{aerosol,noneBC,\downarrow} - F_{aerosol,noneBC,\uparrow}). \quad (9)$$

127 Similarly, the direct radiative forcing of $eBC_{>700}$ ($DRF_{eBC,>700}$) was defined as:

$$128 DRF_{eBC,>700} = (F_{aerosol,\downarrow} - F_{aerosol,\uparrow}) - (F_{aerosol,noneBC,>700,\downarrow} - F_{aerosol,noneBC,>700,\uparrow}), \quad (10)$$

129 where $F_{aerosol,noneBC,>700,\downarrow}$ ($F_{aerosol,noneBC,>700,\uparrow}$) was downward (upward) radiative irradiance flux at TOA with aerosol
130 except $eBC_{>700}$. The contribution of $eBC_{>700}$ to DRF_{eBC} ($f_{DRF,>700}$) was defined as

$$131 f_{DRF,>700} = \frac{DRF_{eBC,>700}}{DRF_{eBC}} \times 100 \%. \quad (11)$$

132 SBDART simulation required information of surface albedo, vertical profiles of meteorological parameters and aerosol
133 optical parameters. Surface albedo was acquired from Moderate Resolution Imaging Spectroradiometer (MODIS)/Terra
134 surface reflectance data with temporal and spatial resolution of 1 d and 0.05° (MOD09CMG). The gridded data around the
135 measurement site was averaged to represent surface albedo of the measurement site.

136 The vertical profile of meteorological parameters included vertical profile of pressure, temperature, water vapor and ozone,
137 which were obtained from the fifth generation ECMWF (European Center for Medium Range Weather Forecasts) reanalysis
138 data for global climate and weather (ERA5). The ERA5 data had temporal and spatial resolution of 1 h and 0.25° with 38
139 vertical layers from surface to about 50 km above surface. At each layer, the gridded data around the measurement site was
140 also averaged to represent meteorological parameters of the measurement site. The time resolution of meteorological
141 parameters was averaged to daily to match that of surface albedo.

142 The vertical profile of aerosol optical parameters included the vertical profile of bulk aerosol extinction coefficient ($\sigma_{ext,bulk}$),
143 single scattering albedo (SSA) and asymmetry factor (g) at different wavelengths, which were parameterized based on the
144 study of Zhao et al. (2019) and described here briefly. The bulk aerosol particle number concentration (N_{bulk}) was
145 parameterized according to aircraft study by Liu et al. (2009). Dry $N_{size-resolved}$ at different heights had the same shape after
146 normalized by corresponding N_{bulk} . The parameterization of $m_{eBC,bulk}$ and eBCMSD was the same as N_{bulk} and dry $N_{size-resolved}$.
147 51% of eBC mass was assumed externally mixed and the rest of eBC mass was assumed internally mixed with core-shell
148 geometry (Ma et al., 2012) in each size bin. For the case of aerosol without eBC-containing particle (larger than 700 nm),
149 eBCMSD (larger than 700 nm) was set to 0. The aerosol optical parameters varying with height-dependent RH were calculated
150 by Mie scattering theory and κ -Kohler theory (Petters and Kreidenweis, 2007) assuming hygroscopic growth parameter of
151 0.22 (Tan et al., 2019). The refractive indices of eBC, water and non-eBC material without water were assumed $1.8 + 0.54i$
152 (Kuang et al., 2015), $1.33 + 10^{-7}i$ and $1.53 + 10^{-7}i$ (Wex et al., 2002), respectively. The refractive index of non-eBC material
153 mixed with water after hygroscopic growth was derived by volume-weighted rule (Wex et al., 2002). With the above
154 information, the vertical profiles of $\sigma_{ext,bulk}$, SSA and g could be calculated. The time resolution of aerosol optical parameters
155 was averaged to daily to match that of surface albedo.



156 **3 Results and discussion**

157 **3.1 Equivalent black carbon mass size distribution**

158 **3.1.1 Overview**

159 eBCMSD measured in Changzhou and Beijing was presented in Fig. 2a and Fig. 2b1 – 2b4, respectively. It could be seen
160 that eBCMSD varied significantly and exhibited diverse patterns in both Changzhou and Beijing. For example, unimodal
161 structure of eBCMSD occurred around December 9th 2021 in Beijing. eBCMSD did not show clear modal structure around
162 June 2nd 2021 in Changzhou and around November 15th in Beijing. For the cases where eBCMSD exhibited modal structure,
163 the peak diameter of the mode could change substantially with increasing pollution, such as from November 2nd 2021 to
164 November 6th 2021 in Beijing. The peak diameter of the mode could also vary without systematical shift, such as from January
165 6th 2022 to January 8th 2022 in Beijing.

166 eBCMSD was presented with normalized probability density function (pdf) to study general characteristics of eBCMSD.
167 Figure 5a1 and 5a2 were the normalized pdf over the whole campaign of Changzhou and Beijing, respectively. It could be
168 seen that eBCMSD in Changzhou was significantly different from that in Beijing. There were two modes in the median of
169 eBCMSD in Changzhou, which peaked at around 240 nm and 1249 nm, respectively. Yu et al. (2010) found 3 modes in
170 ECMSD, namely modes around 300 nm, 1 μm and 5 μm , and named the 3 modes as condensation mode, droplet mode and
171 coarse mode, respectively. Following the nomenclature by Yu et al. (2010), the mode peaking at 240 nm and 1249 nm could
172 be termed as condensation mode and droplet mode, respectively. In contrast, only condensation mode was identified in median
173 eBCMSD in Beijing, which peaked at 427 nm. The variation of eBCMSD, defined as the difference between upper quartile
174 and lower quartile, in Changzhou was overall smaller than that in Beijing. The variation of eBCMSD in Changzhou (Beijing)
175 ranged from 0.52 (0.54) $\mu\text{g m}^{-3}$ to 0.91 (1.73) $\mu\text{g m}^{-3}$ with average value of 0.75 (1.05) $\mu\text{g m}^{-3}$. The maximum upper quartile
176 of eBCMSD in Changzhou was 1.58 $\mu\text{g m}^{-3}$. In comparison, the upper quartile of eBCMSD in Beijing could reached up to
177 2.14 $\mu\text{g m}^{-3}$, indicating the evolution of eBCMSD in Beijing was more drastic than that in Changzhou.

178 **3.1.2 Evolution with respect to pollution level**

179 In order to investigate the evolution of eBCMSD under different pollution stages, eBCMSD was grouped into 3 periods:
180 (1) clean period in which $m_{\text{eBC,bulk}}$ was lower than 0.5 $\mu\text{g m}^{-3}$, (2) transitional period in which $m_{\text{eBC,bulk}}$ was greater than 0.5
181 $\mu\text{g m}^{-3}$ but lower than 1.0 $\mu\text{g m}^{-3}$, (3) polluted period in which $m_{\text{eBC,bulk}}$ was greater than 1.0 $\mu\text{g m}^{-3}$. Data from clean,
182 transitional and polluted period accounted for 22.6 % (30.9 %), 51.3 % (31.9 %) and 26.0 % (37.2 %) of total data in
183 Changzhou (Beijing), respectively, showing that Changzhou (Beijing) was dominated by transitional (polluted) period in this
184 study.

185 In the clean period, there was no distinct difference in eBCMSD between Changzhou (Fig. 5b1) and Beijing (Fig. 5b2).
186 Neither eBCMSD in Changzhou nor eBCMSD in Beijing exhibited obvious modal structure in the size range of measurement.
187 The value of eBCMSD in both Changzhou and Beijing decreased with increasing D_p in general. For Changzhou (Beijing),



188 the median of eBCMSD decreased from 0.87 (0.47) $\mu\text{g m}^{-3}$ at 200 nm to 0.26 (0.26) $\mu\text{g m}^{-3}$ at 1500 nm with average value of
189 0.42 (0.34) $\mu\text{g m}^{-3}$. The variation of eBCMSD in Changzhou (Beijing) was 0.24 (0.24) $\mu\text{g m}^{-3}$ ~ 0.47 (0.55) $\mu\text{g m}^{-3}$ with
190 average value of 0.32 (0.35) $\mu\text{g m}^{-3}$, showing that the variation of eBCMSD in Changzhou was comparable to that in Beijing.

191 As polluted stage evolved to transitional period, the level of eBCMSD increased in both Changzhou (Fig. 5c1) and Beijing
192 (Fig. 5c2) compared to that in clean period. The median eBCMSD reached 0.41 (0.39) $\mu\text{g m}^{-3}$ ~ 1.09 (1.07) $\mu\text{g m}^{-3}$ with
193 average value of 0.75 (0.78) $\mu\text{g m}^{-3}$ in Changzhou (Beijing), respectively, about twice as much as the median eBCMSD in
194 clean period. The variation of eBCMSD in Changzhou (Beijing) reached 0.41 (0.44) $\mu\text{g m}^{-3}$ ~ 0.86 (0.86) $\mu\text{g m}^{-3}$ with average
195 value of 0.53 (0.61) $\mu\text{g m}^{-3}$, about twice as much as that in clean period. It could be seen that the value of median and variation
196 of eBCMSD in Changzhou were comparable to that in Beijing. However, the pattern of eBCMSD in Changzhou was obviously
197 different from that in Beijing. The peak value of median eBCMSD located at 240 (347) nm in Changzhou (Beijing). Median
198 eBCMSD in Changzhou exhibited two modes, namely condensation mode and droplet, with boundary at around 866 nm. In
199 comparison, median eBCMSD in Beijing only had one mode, namely condensation mode. The difference in peak diameter of
200 condensation mode between Changzhou and Beijing was as large as 107 nm. Median eBCMSD at clean period was subtracted
201 from that at transitional period to study eBC mass increment at each D_p , as shown in Fig. 6a1. It could be clearly seen that
202 mass increment in Changzhou peaked at 289 nm and 1249 nm, contributing to condensation mode and droplet mode in
203 eBCMSD, respectively. In contrast, mass increment in Beijing only peaked at 385 nm, contributing to condensation mode in
204 eBCMSD.

205 As the pollution stage came to polluted period, the level of eBCMSD increased drastically in both Changzhou (Fig. 5d1)
206 and Beijing (Fig. 5d2) compared to that in clean period. Both the level and the variation of eBCMSD increased with the
207 development of pollution. The median eBCMSD increased to 0.88 (0.61) ~ 2.12 (2.45) $\mu\text{g m}^{-3}$ with average value of 1.49
208 (1.52) $\mu\text{g m}^{-3}$ in Changzhou (Beijing), about 4 times as much as the median eBCMSD in clean period. The variation of
209 eBCMSD in Changzhou (Beijing) reached 0.60 (0.73) ~ 1.11 (1.06) $\mu\text{g m}^{-3}$ with average value of 0.92 (0.94) $\mu\text{g m}^{-3}$, about 3
210 times as much as that in clean period. The difference in pattern of eBCMSD between Changzhou and Beijing became more
211 distinct. Median eBCMSD in Changzhou clearly exhibited a bimodal structure where the condensation mode and droplet
212 mode peaked at 289 nm and 1249 nm, respectively. Median eBCMSD in Beijing exhibited a unimodal structure where the
213 condensation mode peaked a 527 nm. As shown in Fig. 6b1, the peak of mass increment in Changzhou (Beijing) shifted from
214 289 (385) nm to 347 (527) nm, varied by 58 (142) nm. The significant difference in the shift of peak indicated that aging
215 processes in regional background site was significantly different from that in urban site.

216 **3.1.3 Contribution of equivalent black carbon-containing particle larger than 700 nm to bulk equivalent black carbon** 217 **mass concentration**

218 It could be seen from Fig. 2 that $eBC_{>700}$ was ubiquitous. The median (lower quartile ~ upper quartile) of $m_{eBC,bulk}$ was 0.73
219 (0.52 ~ 1.03) $\mu\text{g m}^{-3}$ in Changzhou and 0.79 (0.43 ~ 1.31) $\mu\text{g m}^{-3}$ in Beijing (Fig. 7a1). The median of $m_{eBC,bulk}$ was comparable



220 between Changzhou and Beijing. The variation of $m_{\text{eBC,bulk}}$ in Changzhou, $0.51 \mu\text{g m}^{-3}$, was smaller than that in Beijing, 0.88
221 $\mu\text{g m}^{-3}$. $m_{\text{eBC,bulk},>700}$ in Changzhou was overall comparable to that in Beijing (Fig. 7a2). $m_{\text{eBC,bulk},>700}$ was 0.20 ($0.13 \sim 0.32$)
222 $\mu\text{g m}^{-3}$ in Changzhou and 0.18 ($0.10 \sim 0.33$) $\mu\text{g m}^{-3}$ in Beijing. Considering that the variation of $m_{\text{eBC,bulk},>700}$ in Changzhou,
223 $0.19 \mu\text{g m}^{-3}$, was comparable to that in Beijing, $0.23 \mu\text{g m}^{-3}$, the larger variation in $m_{\text{eBC,bulk}}$ in Beijing was mainly from eBC-
224 containing particles less than 700 nm . $f_{\text{m},>700}$ was 27.8 ($20.9 \sim 36.5$) % in Changzhou and 24.1 ($17.5 \sim 34.2$) % in Beijing (Fig.
225 7a3), indicating that $\text{eBC}_{>700}$ was overall one quarter of $m_{\text{eBC,bulk}}$. $f_{\text{m},>700}$ in Changzhou was slightly larger than that in Beijing,
226 which was contributed by droplet mode of eBCMSD in Changzhou.

227 The statistics of mass contribution of $\text{eBC}_{>700}$ were studied with different pollution stages. As shown in Fig. 7a1, $m_{\text{eBC,bulk}}$
228 increased from 0.41 ($0.33 \sim 0.45$) $\mu\text{g m}^{-3}$ in clean period through 0.71 ($0.58 \sim 0.83$) $\mu\text{g m}^{-3}$ in transitional period to 1.33 (1.16
229 ~ 1.71) $\mu\text{g m}^{-3}$ in polluted period by 3.2 times in Changzhou and increased from 0.32 ($0.22 \sim 0.41$) $\mu\text{g m}^{-3}$ in clean period
230 through 0.73 ($0.61 \sim 0.85$) $\mu\text{g m}^{-3}$ in transitional period to 1.47 ($1.21 \sim 1.82$) $\mu\text{g m}^{-3}$ in polluted period by 4.6 times in Beijing.
231 As shown in Fig. 7a2, the change of $m_{\text{eBC,bulk},>700}$ with pollution level was substantial in both Changzhou and Beijing. For
232 Changzhou, $m_{\text{eBC,bulk},>700}$ increased from 0.11 ($0.07 \sim 0.15$) $\mu\text{g m}^{-3}$ in clean period to 0.20 ($0.14 \sim 0.27$) $\mu\text{g m}^{-3}$ in transition
233 period, and reached 0.40 ($0.29 \sim 0.50$) $\mu\text{g m}^{-3}$ in polluted period, increasing by as large as 3.6 times from clean period to
234 polluted period. For Beijing, $m_{\text{eBC,bulk},>700}$ increased from 0.07 ($0.05 \sim 0.12$) $\mu\text{g m}^{-3}$ in clean period to 0.17 ($0.11 \sim 0.23$) μg
235 m^{-3} in transition period, and reached 0.36 ($0.25 \sim 0.52$) $\mu\text{g m}^{-3}$ in polluted period, increasing by as large as 5.1 times from
236 clean period to polluted period. The change in $m_{\text{eBC,bulk}}$ and $m_{\text{eBC,bulk},>700}$ was overall consistent with the development of
237 pollution, leading to unobvious change in $f_{\text{m},>700}$ (Fig. 7a3). $f_{\text{m},>700}$ in Changzhou changed from 28.5 ($20.3 \sim 36.0$) % in
238 clean period through 28.4 ($20.7 \sim 36.9$) % in transitional period to 27.4 ($22.6 \sim 36.2$) % in polluted period. $f_{\text{m},>700}$ in Beijing
239 varied from 26.2 ($18.4 \sim 36.8$) % in clean period through 22.8 ($16.3 \sim 32.3$) % in transitional period to 23.8 ($18.1 \sim 31.9$) %
240 in polluted period.

241 3.1.4 Diurnal cycle

242 It could be seen clearly that the level of eBCMSD during daytime was overall lower than that during nighttime in both
243 Changzhou (Fig. 8a1) and Beijing (Fig. 8a2), showing that eBCMSD was significantly regulated by planetary boundary layer.
244 For Changzhou (Beijing), eBCMSD from 10:00 to 18:00 (08:00 to 18:00) was obviously lower than from 20:00 to 06:00
245 (20:00 to 06:00). Accordingly, $m_{\text{eBC,bulk}}$ in Changzhou reached minimum of 0.56 ($0.48 \sim 0.88$) $\mu\text{g m}^{-3}$ at 12:00 and maximum
246 of 0.97 ($0.80 \sim 1.24$) $\mu\text{g m}^{-3}$ at 21:00 (Fig. 8b1). $m_{\text{eBC,bulk}}$ in Beijing reached minimum of 0.65 ($0.42 \sim 1.02$) $\mu\text{g m}^{-3}$ at 14:00
247 and maximum of 1.08 ($0.55 \sim 1.52$) $\mu\text{g m}^{-3}$ at 00:00, (Fig. 8b2). The apparent diurnal cycle was found in the condensation
248 mode of eBCMSD, which was mostly less than 700 nm . In contrast, diurnal cycle was not obvious for eBCMSD larger than
249 700 nm for both Changzhou and Beijing. Consequently, neither $m_{\text{eBC,bulk},>700}$ in Changzhou (Fig. 8c1) nor $m_{\text{eBC,bulk},>700}$ in
250 Beijing (Fig. 8c2) exhibited obvious diurnal cycle. $m_{\text{eBC,bulk},>700}$ in both Changzhou and Beijing fluctuated around $0.2 \mu\text{g m}^{-3}$
251 ³, consistent with Sect. 3.1.3. Combining the diurnal variation of $m_{\text{eBC,bulk}}$ and $m_{\text{eBC,bulk},>700}$, $f_{\text{m},>700}$ was negatively correlated



252 to $m_{eBC,bulk}$ according to Eq. (3) with higher value during the daytime and lower value during the nighttime. $f_{m,>700}$ reached
253 maximum of 35.4 (26.6 ~ 41.1) % at 09:00 and reached minimum of 23.6 (13.9 ~ 30.8) % at 21:00 in Changzhou (Fig. 8d1).
254 $f_{m,>700}$ reached maximum of 31.0 (20.8 ~ 36.9) % at 15:00 and reached minimum of 23.5 (16.1 ~ 27.8) % at 01:00 in Beijing
255 (Fig. 8d2).

256 3.2 Size-resolved absorption coefficient

257 3.2.1 Overview

258 The timeseries of $\sigma_{ab,size-resolved}$ in Changzhou and Beijing were plotted in Fig. 3a and Fig. 3b1 – 3b4, respectively. $\sigma_{ab,size-}$
259 resolved varied substantially with D_p , time and location. In general, $\sigma_{ab,size-resolved}$ exhibited a unimodal structure with lower
260 value less than 5 Mm^{-1} at the edge of D_p spectrum and higher value larger than 20 Mm^{-1} in between. The large spread of BC
261 absorption with respect to D_p clearly highlighted the important role of particle size on absorption. The peak diameter of $\sigma_{ab,size-}$
262 resolved could vary with time. For instance, from December 9th 2021 to December 10th 2021 in Beijing and from January 22nd
263 2022 to January 25th 2022 in Beijing, the peak diameter of $\sigma_{ab,size-resolved}$ shifted clearly from about 400 nm to about 600 nm
264 and from about 500 nm to about 800 nm, respectively. The peak diameter of $\sigma_{ab,size-resolved}$ could also vary without systematical
265 change, such as $\sigma_{ab,size-resolved}$ in Changzhou and from January 6th 2022 to January 8th 2022 in Beijing. The complicated
266 variation of $\sigma_{ab,size-resolved}$ with time manifested complex mechanism influencing evolution of BC absorption.

267 The general characteristics of $\sigma_{ab,size-resolved}$ in Changzhou and Beijing was shown in Fig. 5a3 and Fig. 5a4, respectively.
268 The median $\sigma_{ab,size-resolved}$ in both Changzhou and Beijing both exhibited unimodal structure. For Changzhou (Beijing), $\sigma_{ab,size-}$
269 resolved had maximum value of 7.88 (10.59) Mm^{-1} at 416.1 (427.2) nm and minimum value of 1.63 (2.90) Mm^{-1} at 1500 (1500)
270 nm with average value of 5.39 (6.21) Mm^{-1} . The maximum value was 4.9 (3.7) times as large as minimum value in Changzhou
271 (Beijing), showing the significant dependence of absorption on particle size. D_p which had higher median value of $\sigma_{ab,size-}$
272 resolved corresponded to larger variation on the whole. The variation of $\sigma_{ab,size-resolved}$ ranged from 2.25 (2.82) Mm^{-1} at 1500
273 (1500) nm to 7.43 (17.90) Mm^{-1} at 500 (527) nm with average value of 4.99 (8.97) Mm^{-1} in Changzhou (Beijing). The
274 variation of $\sigma_{ab,size-resolved}$ was as large as the level of $\sigma_{ab,size-resolved}$ in both Beijing and Changzhou, showing the large
275 variability of BC absorption. The variation of $\sigma_{ab,size-resolved}$ in Beijing was overall 1.8 times as large as that in Changzhou,
276 indicating that the evolution of $\sigma_{ab,size-resolved}$ in different sites could be significantly different.

277 3.2.2 Evolution with respect to pollution level

278 $\sigma_{ab,size-resolved}$ was grouped into 3 periods based on $m_{eBC,bulk}$ as described in Sect. 3.1.2. In clean period, the value of $\sigma_{ab,size-}$
279 resolved overall decreased with increasing D_p in both Changzhou (Fig. 5b3) and Beijing (Fig. 5b4), and the pattern of $\sigma_{ab,size-}$
280 resolved had no obvious modal structure. In Changzhou (Beijing), the value of $\sigma_{ab,size-resolved}$ decreased from 4.67 (3.43) Mm^{-1} at
281 200 (427) nm to 0.88 (1.80) Mm^{-1} at 1500 (1500) nm with average value of 2.95 (2.49) Mm^{-1} . The variation of $\sigma_{ab,size-resolved}$
282 in Changzhou (Beijing) ranged from 1.06 (1.57) Mm^{-1} to 2.72 (3.12) Mm^{-1} with average value of 2.04 (2.47) Mm^{-1} .

283 During the transitional period, the unimodal pattern could be identified in both Changzhou (Fig. 5c3) and Beijing (Fig.



284 5c4). Median $\sigma_{\text{ab,size-resolved}}$ peaked at 416 (427) nm with value of 7.80 (10.04) Mm^{-1} in Changzhou (Beijing). Median $\sigma_{\text{ab,size-}}$
285 resolved in clean period was subtracted from that in transitional period to study absorption increment at each D_p , as shown in
286 Fig. 6a2. The increment of $\sigma_{\text{ab,size-resolved}}$ in Changzhou (Beijing) had maximum value of 3.94 (6.61) Mm^{-1} at 416 (427) nm
287 and minimum value of 0.66 (1.15) Mm^{-1} at 1500 (1500) nm. The increment of absorption was most at around 420 nm and
288 least at 1500 nm, showing the significant difference in the change of absorption at different D_p with the development of
289 pollution. The maximum increment of absorption in Beijing was 1.7 times as large as that in Changzhou. Hence, the evolution
290 of absorption could be different substantially in different locations. The variation of $\sigma_{\text{ab,size-resolved}}$ in Changzhou (Beijing)
291 ranged from 1.94 (2.32) Mm^{-1} to 4.03 (6.43) Mm^{-1} with average value of 3.08 (4.45) Mm^{-1} , increasing by about 1.5 times
292 compared to clean period.

293 In the polluted period, the unimodal pattern of $\sigma_{\text{ab,size-resolved}}$ was significant in both Changzhou (Fig. 5d3) and Beijing (Fig.
294 5d4). Median $\sigma_{\text{ab,size-resolved}}$ peaked at 416 (527) nm with value of 16.79 (25.85) Mm^{-1} and had minimum value of 2.85 (4.23)
295 Mm^{-1} at 1500 (1500) nm in Changzhou (Beijing). Compared to transition period, peak diameter remained unchanged in
296 Changzhou but increased by 100 nm in Beijing, indicating the evolution of $\sigma_{\text{ab,size-resolved}}$ with aging process was different
297 between regional background site and typical urban site. The increment of absorption in Changzhou (Beijing) was most
298 significant at 416 (527) nm with value of 12.93 (22.94) Mm^{-1} and least at 1500 (1500) nm with value of 1.97 (2.44) Mm^{-1} , as
299 shown in Fig. 6b2. It could be seen that the diameter of increment in absorption remain unchanged in Changzhou and shifted
300 by 100 nm in Beijing, indicating that absorption at different D_p varied differently at different locations with the deterioration
301 of pollution. The variation of $\sigma_{\text{ab,size-resolved}}$ in Changzhou (Beijing) ranged from 2.19 (3.82) Mm^{-1} to 9.05 (15.61) Mm^{-1} with
302 average value of 5.72 (8.22) Mm^{-1} , increasing by about 3 times compared to clean period, indicating that the variability of
303 $\sigma_{\text{ab,size-resolved}}$ increased with the development of pollution.

304 3.2.3 Contribution of equivalent black carbon-containing particle larger than 700 nm to bulk absorption coefficient

305 It could be seen from the timeseries of $\sigma_{\text{ab,size-resolved}}$ in both Changzhou (Fig. 3a) and Beijing (Fig. 3b1 – 3b4) that
306 absorption of $\text{eBC}_{>700}$ was nonnegligible. $\sigma_{\text{ab,bulk}}$ was 4.93 (3.53 ~ 7.24) Mm^{-1} in Changzhou and 6.37 (3.31 ~ 11.68) Mm^{-1}
307 in Beijing on the whole, as shown in Fig. 7b1. Both median and variation of $\sigma_{\text{ab,bulk}}$ in Changzhou were less than that in
308 Beijing. $\sigma_{\text{ab,bulk,>700}}$ was 1.03 (0.62 ~ 1.59) Mm^{-1} in Changzhou, accounting for 19.6 (15.8 ~ 24.6) % of $\sigma_{\text{ab,bulk}}$, and 1.47 (0.81
309 ~ 2.83) Mm^{-1} in Beijing, accounting for 25.9 (19.6 ~ 33.7) % of $\sigma_{\text{ab,bulk}}$, respectively, as shown in Fig. 7b2 and Fig. 7b3. It
310 could be clearly seen that $\text{eBC}_{>700}$ contributed to substantial part of total absorption, and should be explicitly considered in
311 BC radiative estimation.

312 With the aggravation of pollution, the change of $m_{\text{eBC,bulk}}$ in Changzhou was overall in agreement with that in Beijing (Fig.
313 7a1). However, the change of $\sigma_{\text{ab,bulk}}$ with the development of pollution was different between Changzhou and Beijing (Fig.
314 4b1). In the clean period, $\sigma_{\text{ab,bulk}}$ in Changzhou with value of 2.71 (2.30 ~ 3.28) Mm^{-1} was comparable to that in Beijing with
315 value of 2.47 (1.65 ~ 3.28) Mm^{-1} . In the transitional period, $\sigma_{\text{ab,bulk}}$ was 4.83 (4.04 ~ 6.02) Mm^{-1} in Changzhou and 5.93 (4.72



316 ~ 7.33) Mm^{-1} in Beijing. The deviation in $\sigma_{\text{ab,bulk}}$ was about 1 Mm^{-1} between Changzhou and Beijing. In the polluted period,
317 $\sigma_{\text{ab,bulk}}$ was 9.61 ($7.99 \sim 11.93$) Mm^{-1} in Changzhou and 13.65 ($10.94 \sim 17.59$) Mm^{-1} in Beijing. The deviation in $\sigma_{\text{ab,bulk}}$ came
318 to 4 Mm^{-1} between Changzhou and Beijing. It could be seen that with the development of pollution, the change of $\sigma_{\text{ab,bulk}}$ in
319 Changzhou was less than that in Beijing. MAC_{bulk} , defined as the ratio of median $\sigma_{\text{ab,bulk}}$ to median $m_{\text{eBC,bulk}}$, changed from
320 6.61 (7.72) $\text{m}^2 \text{ g}^{-1}$ through 6.80 (8.13) $\text{m}^2 \text{ g}^{-1}$ to 7.23 (9.29) $\text{m}^2 \text{ g}^{-1}$ in Changzhou (Beijing). The increase in MAC_{bulk} in both
321 Changzhou and Beijing with the aggravation of pollution indicated the aging of BC. MAC_{bulk} in Changzhou was overall lower
322 than that in Beijing and increased slower than that in Beijing with the development of pollution, indicating that the BC
323 properties and aging process in Changzhou differentiate from that in Beijing.

324 $\sigma_{\text{ab,bulk},>700}$ in both Changzhou and Beijing increased with the development of pollution, as shown in Fig. 7b2. $\sigma_{\text{ab,bulk},>700}$
325 increased from 0.54 ($0.62 \sim 1.59$) Mm^{-1} through 0.96 ($0.72 \sim 1.32$) Mm^{-1} to 1.75 ($1.53 \sim 2.36$) Mm^{-1} in Changzhou and
326 increased from 0.63 ($0.43 \sim 0.91$) Mm^{-1} through 1.36 ($1.01 \sim 1.79$) Mm^{-1} to 3.45 ($2.46 \sim 5.34$) Mm^{-1} in Beijing. $\sigma_{\text{ab,bulk},>700}$
327 increased by 3.2 (5.5) times in Changzhou (Beijing). The relative increase of $\sigma_{\text{ab,bulk},>700}$ was overall consistent with that of
328 $\sigma_{\text{ab,bulk}}$ in both Changzhou and Beijing. As a result, there was no significant change in $f_{\text{ab},>700}$ with the development of pollution
329 (Fig. 7b3). $f_{\text{ab},>700}$ varied from 19.8 ($15.2 \sim 23.8$) % through 19.3 ($15.9 \sim 25.3$) % to 19.6 ($15.5 \sim 24.5$) % in Changzhou and
330 varied from 27.9 ($20.7 \sim 36.4$) % through 23.2 ($17.8 \sim 30.7$) % to 26.7 ($20.4 \sim 34.7$) % in Changzhou. It could be seen that
331 the increase of $\sigma_{\text{ab,bulk},>700}$ in Changzhou was less than that in Beijing with the development of pollution. Specifically,
332 $\sigma_{\text{ab,bulk},>700}$ in Beijing was 2.0 times larger than that in Changzhou, showing that the change of $\sigma_{\text{ab,bulk},>700}$ with the aggravation
333 of pollution could be different significantly in different sites.

334 3.2.4 Diurnal cycle

335 $\sigma_{\text{ab,size-resolved}}$ exhibited clear diurnal cycle in both Changzhou (Fig. 8a3) and Beijing (Fig. 8a4) with lower value of $\sigma_{\text{ab,size-}}$
336 resolved during daytime and higher value during nighttime. Accordingly, $\sigma_{\text{ab,bulk}}$ had minimum value of 3.51 ($3.16 \sim 4.26$) Mm^{-1}
337 1 at 14:00 and maximum value of 7.20 ($3.80 \sim 10.58$) Mm^{-1} at 01:00 in Changzhou (Fig. 8b3). $\sigma_{\text{ab,bulk}}$ had minimum value of
338 3.96 ($2.97 \sim 9.10$) Mm^{-1} at 14:00 and maximum value of 7.86 ($4.04 \sim 13.19$) Mm^{-1} at 00:00 in Beijing (Fig. 8b4), reflecting
339 the regulation by planetary boundary layer. In contrast, neither $\sigma_{\text{ab,bulk},>700}$ in Changzhou (Fig. 8c3) nor $\sigma_{\text{ab,bulk},>700}$ in Beijing
340 (Fig. 8c4) exhibited obvious diurnal cycle. Therefore, $f_{\text{ab},>700}$, inversely proportional to $\sigma_{\text{ab,bulk}}$, had higher value during
341 daytime and lower value during nighttime. For Changzhou, $f_{\text{ab},>700}$ reached maximum at 09:00 with value of 25.3 ($20.4 \sim$
342 27.4) % and came to minimum at 21:00 with value of 16.6 ($13.0 \sim 19.6$) % (Fig. 8d3). For Beijing, $f_{\text{ab},>700}$ reached maximum
343 at 10:00 with value of 30.4 ($21.1 \sim 36.3$) % and came to minimum at 01:00 with value of 24.5 ($17.2 \sim 28.1$) % (Fig. 8d4).

344 3.3 Direct radiative forcing of equivalent black carbon

345 3.3.1 Overview

346 The timeseries of DRF_{eBC} in Changzhou and Beijing was shown in Fig. 4a1 and Fig. 4b1 – 4b4, respectively. It could be
347 seen that DRF_{eBC} varied significantly in both Changzhou and Beijing. DRF_{eBC} was estimated to be 0.93 ($0.70 \sim 1.39$) W m^{-2}



348 in Changzhou and 1.10 ($0.65 \sim 2.00$) W m^{-2} in Beijing, respectively (Fig. 7c1). The variation of DRF_{eBC} was as large as the
349 median value of DRF_{eBC} , clearly indicating the large variability of BC radiative effect. DRF_{eBC} increased substantially with
350 the aggravation of pollution (Fig. 7c1). DRF_{eBC} increased from 0.38 ($0.38 \sim 0.38$) W m^{-2} through 0.77 ($0.70 \sim 0.98$) W m^{-2} to
351 1.67 ($1.29 \sim 2.07$) W m^{-2} by 4.4 times in Changzhou and from 0.42 ($0.33 \sim 0.66$) W m^{-2} through 1.17 ($0.79 \sim 1.45$) W m^{-2} to
352 2.41 ($1.68 \sim 2.86$) W m^{-2} by 5.7 times in Beijing with the development of pollution.

353 3.3.2 Contribution of equivalent black carbon-containing particle larger than 700 nm to direct radiative forcing of 354 equivalent black carbon

355 $\text{DRF}_{\text{eBC},>700}$ was estimated to be 0.19 ($0.13 \sim 0.26$) W m^{-2} in Changzhou and 0.20 ($0.13 \sim 0.37$) W m^{-2} in Beijing (Fig. 7c2),
356 respectively, which accounted for 20.5 (18.4 ~ 22.2) % and 21.0 (16.3 ~ 26.1) % of DRF_{eBC} (Fig. 7c3), respectively. Therefore,
357 $\text{eBC}_{>700}$ contributed to an important portion of BC radiative effect. With the aggravation of pollution, $\text{DRF}_{\text{eBC},>700}$ increased
358 substantially and was different regionally (Fig. 7c2), $\text{DRF}_{\text{eBC},>700}$ increased from 0.10 ($0.10 \sim 0.10$) W m^{-2} through 0.17 (0.12
359 ~ 0.26) W m^{-2} to 0.24 ($0.22 \sim 0.30$) W m^{-2} by 2.4 times in Changzhou and from 0.10 ($0.08 \sim 0.12$) W m^{-2} through 0.20 (0.17
360 ~ 0.24) W m^{-2} to 0.47 ($0.34 \sim 0.71$) W m^{-2} by 4.7 times in Beijing. The characteristics of $f_{\text{DRF},>700}$ with increasing pollution
361 was complicated (Fig. 7c3). $f_{\text{DRF},>700}$ varied from 25.0 (25.0 ~ 25.0) % through 21.1 (20.3 ~ 22.3) % to 17.6 (15.5 ~ 18.9) %
362 in Changzhou, exhibiting a decreasing trend. However, $f_{\text{DRF},>700}$ varied from 24.4 (17.4 ~ 27.7) % through 18.4 (15.4 ~ 24.5) %
363 to 21.5 (19.1 ~ 26.9) % in Changzhou, without systematical change.

364 3.4 Case study

365 Figure 8 exhibited a pollution episode from October 31st, 2021 to November 6, 2021 in Beijing, which was used for case
366 study to illustrate the large variability of $\text{eBC}_{>700}$. The mean diameter (\bar{D}_p) of eBCMSD was defined as

$$367 \log \bar{D}_p = \frac{\int \log D_p \frac{dm_{\text{eBC}}}{d \log D_p} d \log D_p}{\int \frac{dm_{\text{eBC}}}{d \log D_p} d \log D_p}, \quad (12)$$

368 which was used to depict the spectral variation of eBCMSD because eBCMSD did not always had an explicit modal pattern
369 as mentioned in Sect. 3.1.1, and the corresponding peak diameter was not always easy to be distinguished.

370 With the development of pollution, \bar{D}_p shifted apparently from around 400 nm to around 600 nm (Fig. 9a). $m_{\text{eBC,bulk}}$
371 ($m_{\text{eBC,bulk},>700}$) increased from less than 0.5 (0.15) $\mu\text{g m}^{-3}$ to as large as 2.5 (1.0) $\mu\text{g m}^{-3}$ by 5.0 (6.6) times. $\sigma_{\text{ab,bulk}}$ ($\sigma_{\text{ab,bulk},>700}$)
372 increased from less than 4 (1) Mm^{-1} to as large as 25 (10) Mm^{-1} by 6.3 (10.0) times. DRF_{eBC} ($\text{DRF}_{\text{eBC},>700}$) increased from 1
373 (0.2) W m^{-2} to as large as 4 (1) W m^{-2} by 4.0 (5.0) times. It could be seen that the variability of $\text{eBC}_{>700}$ was significant. $f_{\text{m},>700}$,
374 $f_{\text{ab},>700}$ and $f_{\text{DRF},>700}$ increased from about 20 %, 20 % and 20 % to as large as 50 %, 50 % and 40 %, respectively (Fig. 9b),
375 clearly showing important role of $\text{eBC}_{>700}$ in BC mass, absorption as well as radiative effect.

376 4 Conclusions

377 Black carbon (BC) mass size distribution (BCMSD) was an important factor influencing environmental and radiative effect
378 of BC. However, current BCMSD measurements mainly focused on BC-containing particle less than 700 nm. The



379 characteristics of BC-containing particle greater than 700 nm ($BC_{>700}$) remained uncertain due to limit in technique. In this
380 study, the characteristics of equivalent $BC_{>700}$ ($eBC_{>700}$) were measured and studied based on field measurements in eastern
381 China.

382 Equivalent BCMSD ($eBCMSD$) was measured from 150 nm up to 1.5 μm with time resolution of 1 hour based on the
383 method proposed by Zhao et al. (2022), where $eBCMSD$ was determined by an aerodynamic aerosol classifier (AAC) in
384 tandem with an aethalometer (model AE33, AAC – AE33) and size-resolved particle number concentration was measured
385 concurrently to model the influence of particle size on mass absorption cross section (Zhao et al., 2021). AAC – AE33 was
386 applied to two field measurements in eastern China, namely Changzhou located in the Yangtze River Delta from May 17th to
387 June 3rd in 2021 and Beijing located in the North China Plain from October 29th 2021 to January 26th 2022. Changzhou was
388 a regional background site and Beijing was a typical urban site. The direct radiative forcing of eBC (DRF_{eBC}) was estimated
389 by Santa Barbara DISORT (discrete ordinates radiative transfer) atmospheric radiative transfer (SBDART) model (Ricchiazzi
390 et al., 1998).

391 $eBCMSD$ was different between Changzhou and Beijing. Campaign-averaged $eBCMSD$ in Changzhou exhibited two
392 modes, peaking at 240 nm and 1249 nm, respectively. In contrast, campaign-averaged $eBCMSD$ in Beijing exhibited one
393 mode, peaking at 427 nm. $eBC_{>700}$ was ubiquitous in both Changzhou and Beijing. The campaign-averaged mass, absorption
394 as well as radiative contribution of $eBC_{>700}$ to bulk eBC mass concentration ($m_{eBC,bulk}$), bulk absorption coefficient ($\sigma_{ab,bulk}$),
395 as well as DRF_{eBC} in Changzhou and Beijing were 27.8 (20.9 ~ 36.5) % and 24.1 (17.5 ~ 34.2) %, 19.6 (15.8 ~ 24.6) % and
396 25.9 (19.6 ~ 33.7) %, as well as 20.5 (18.4 ~ 22.2) % and 21.0 (16.3 ~ 26.1) %, respectively, manifesting the important role
397 of $eBC_{>700}$ in environment and climate. Both $eBCMSD$ and size-resolved absorption coefficient ($\sigma_{ab,size-resolved}$) exhibited
398 diurnal variation with lower value during the daytime and higher value during the nighttime in both Changzhou and Beijing.

399 With the aggravation of pollution, the evolution of $eBCMSD$ and $\sigma_{ab,size-resolved}$ in Changzhou was significantly different
400 from that in Beijing. The peak diameter of $eBCMSD$ shifted from 240 (347) nm to 289 (527) nm in Changzhou (Beijing) and
401 the peak diameter of $\sigma_{ab,size-resolved}$ shifted from 416 (427) nm to 416 (527) nm in Changzhou (Beijing), indicating the aging
402 process in regional background site was distinct from that in urban site. Both the level of $eBCMSD$ and $\sigma_{ab,size-resolved}$ increased
403 with the development of pollution in both Changzhou and Beijing. Accordingly, $m_{eBC,bulk}$, $\sigma_{ab,bulk}$ and DRF_{eBC} in Changzhou
404 (Beijing) increased by 3.2 (4.6) times, 3.5 (5.5) times and 4.4 (5.7) times, respectively. $m_{eBC,bulk}$, $\sigma_{ab,bulk}$ and DRF_{eBC} of $eBC_{>700}$
405 in Changzhou (Beijing) increased by 3.6 (5.1) times, 3.2 (5.5) times and 2.4 (4.7) times, respectively, clearly showing the
406 large variation of $eBC_{>700}$. Case study exhibited that contribution of $eBC_{>700}$ to $m_{eBC,bulk}$, $\sigma_{ab,bulk}$ and DRF_{eBC} could increase
407 from 20 % to 50 %, from about 20 % to 50 % and from 20 % to 40 %, respectively. Therefore, it was highly recommended to
408 take $BC_{>700}$ into account in both BC field measurement and model evaluation of BC climate effect.

409 Code and data availability

410 The code and measurement data involved in this study are available upon request to the authors. The data involved in this study is



411 also available online at: https://pan.baidu.com/s/1IE2lyPg0vb8O_GPT1-dSog?pwd=pzi8.

412 **Author contribution**

413 CZ determined the main goal of this study. WZ carried experiments out and prepared the paper with contributions from all co-
414 authors.

415 **Competing interests**

416 The authors declare that they have no conflict of interest.

417 **References**

418 Artaxo, P., Fernandes, E. T., Martins, J. V., Yamasoe, M. A., Hobbs, P. V., Maenhaut, W., Longo, K. M., and Castanho, A.: Large-
419 scale aerosol source apportionment in Amazonia, *J. Geophys. Res.-Atmos.*, 103, 31837-31847, 10.1029/98jd02346, 1998.

420 Berner, A., Reischl, G., and Puxbaum, H.: Size distribution of traffic derived aerosols, *Sci. Total Environ.*, 36, 299-303,
421 10.1016/0048-9697(84)90280-8, 1984.

422 Bond, T. C.: Spectral dependence of visible light absorption by carbonaceous particles emitted from coal combustion, *Geophys. Res.*
423 *Lett.*, 28, 4075-4078, 10.1029/2001gl013652, 2001.

424 Bond, T. C., Streets, D. G., Yarber, K. F., Nelson, S. M., Woo, J. H., and Klimont, Z.: A technology-based global inventory of black
425 and organic carbon emissions from combustion, *J. Geophys. Res.-Atmos.*, 109, 43, 10.1029/2003jd003697, 2004.

426 Bond, T. C., and Bergstrom, R. W.: Light absorption by carbonaceous particles: An investigative review, *Aerosol Science and*
427 *Technology*, 40, 27-67, 10.1080/02786820500421521, 2006.

428 Bond, T. C., Doherty, S. J., Fahey, D. W., Forster, P. M., Berntsen, T., DeAngelo, B. J., Flanner, M. G., Ghan, S., Karcher, B., Koch,
429 D., Kinne, S., Kondo, Y., Quinn, P. K., Sarofim, M. C., Schultz, M. G., Schulz, M., Venkataraman, C., Zhang, H., Zhang, S., Bellouin,
430 N., Guttikunda, S. K., Hopke, P. K., Jacobson, M. Z., Kaiser, J. W., Klimont, Z., Lohmann, U., Schwarz, J. P., Shindell, D., Storelvmo,
431 T., Warren, S. G., and Zender, C. S.: Bounding the role of black carbon in the climate system: A scientific assessment, *J. Geophys.*
432 *Res.-Atmos.*, 118, 5380-5552, 10.1002/jgrd.50171, 2013.

433 Chow, J. C., Watson, J. G., Crow, D., Lowenthal, D. H., and Merrifield, T.: Comparison of IMPROVE and NIOSH Carbon
434 Measurements, *Aerosol Science and Technology*, 34, 23-34, 10.1080/02786820119073, 2001.

435 Drinovec, L., Mocnik, G., Zotter, P., Prevot, A. S. H., Ruckstuhl, C., Coz, E., Rupakheti, M., Sciare, J., Muller, T., Wiedensohler,
436 A., and Hansen, A. D. A.: The "dual-spot" Aethalometer: an improved measurement of aerosol black carbon with real-time loading
437 compensation, *Atmospheric Measurement Techniques*, 8, 1965-1979, 10.5194/amt-8-1965-2015, 2015.

438 Fuller, K. A., Malm, W. C., and Kreidenweis, S. M.: Effects of mixing on extinction by carbonaceous particles, *J. Geophys. Res.-*
439 *Atmos.*, 104, 15941-15954, 10.1029/1998jd100069, 1999.

440 Guo, Y. H.: Characteristics of size-segregated carbonaceous aerosols in the Beijing-Tianjin-Hebei region, *Environmental Science*
441 *and Pollution Research*, 23, 13918-13930, 10.1007/s11356-016-6538-z, 2016.

442 Johnson, T. J., Irwin, M., Symonds, J. P. R., Olfert, J. S., and Boies, A. M.: Measuring aerosol size distributions with the aerodynamic



- 443 aerosol classifier, *Aerosol Science and Technology*, 52, 655-665, 10.1080/02786826.2018.1440063, 2018.
- 444 Kuang, Y., Zhao, C. S., Tao, J. C., and Ma, N.: Diurnal variations of aerosol optical properties in the North China Plain and their
445 influences on the estimates of direct aerosol radiative effect, *Atmospheric Chemistry and Physics*, 15, 5761-5772, 10.5194/acp-15-
446 5761-2015, 2015.
- 447 Liu, D. T., Whitehead, J., Alfarra, M. R., Reyes-Villegas, E., Spracklen, D. V., Reddington, C. L., Kong, S. F., Williams, P. I., Ting,
448 Y. C., Haslett, S., Taylor, J. W., Flynn, M. J., Morgan, W. T., McFiggans, G., Coe, H., and Allan, J. D.: Black-carbon absorption
449 enhancement in the atmosphere determined by particle mixing state, *Nature Geoscience*, 10, 184-U132, 10.1038/ngeo2901, 2017.
- 450 Liu, P. F., Zhao, C. S., Zhang, Q., Deng, Z. Z., Huang, M. Y., Ma, X. C., and Tie, X. X.: Aircraft study of aerosol vertical distributions
451 over Beijing and their optical properties, *Tellus Ser. B-Chem. Phys. Meteorol.*, 61, 756-767, 10.1111/j.1600-0889.2009.00440.x,
452 2009.
- 453 Ma, N., Zhao, C. S., Muller, T., Cheng, Y. F., Liu, P. F., Deng, Z. Z., Xu, W. Y., Ran, L., Nekat, B., van Pinxteren, D., Gnauk, T.,
454 Mueller, K., Herrmann, H., Yan, P., Zhou, X. J., and Wiedensohler, A.: A new method to determine the mixing state of light absorbing
455 carbonaceous using the measured aerosol optical properties and number size distributions, *Atmospheric Chemistry and Physics*, 12,
456 2381-2397, 10.5194/acp-12-2381-2012, 2012.
- 457 Matsui, H., Hamilton, D. S., and Mahowald, N. M.: Black carbon radiative effects highly sensitive to emitted particle size when
458 resolving mixing-state diversity, *Nature Communications*, 9, 10.1038/s41467-018-05635-1, 2018.
- 459 Moosmuller, H., Chakrabarty, R. K., and Arnott, W. P.: Aerosol light absorption and its measurement: A review, *Journal of*
460 *Quantitative Spectroscopy & Radiative Transfer*, 110, 844-878, 10.1016/j.jqsrt.2009.02.035, 2009.
- 461 Peng, J. F., Hu, M., Guo, S., Du, Z. F., Zheng, J., Shang, D. J., Zamora, M. L., Zeng, L. M., Shao, M., Wu, Y. S., Zheng, J., Wang,
462 Y., Glen, C. R., Collins, D. R., Molina, M. J., and Zhang, R. Y.: Markedly enhanced absorption and direct radiative forcing of black
463 carbon under polluted urban environments, *Proceedings of the National Academy of Sciences of the United States of America*, 113,
464 4266-4271, 10.1073/pnas.1602310113, 2016.
- 465 Petters, M. D., and Kreidenweis, S. M.: A single parameter representation of hygroscopic growth and cloud condensation nucleus
466 activity, *Atmospheric Chemistry and Physics*, 7, 1961-1971, 10.5194/acp-7-1961-2007, 2007.
- 467 Petzold, A., Ogren, J. A., Fiebig, M., Laj, P., Li, S. M., Baltensperger, U., Holzer-Popp, T., Kinne, S., Pappalardo, G., Sugimoto, N.,
468 Wehrli, C., Wiedensohler, A., and Zhang, X. Y.: Recommendations for reporting "black carbon" measurements, *Atmospheric*
469 *Chemistry and Physics*, 13, 8365-8379, 10.5194/acp-13-8365-2013, 2013.
- 470 Ramachandran, S., and Rajesh, T. A.: Black carbon aerosol mass concentrations over Ahmedabad, an urban location in western
471 India: Comparison with urban sites in Asia, Europe, Canada, and the United States, *J. Geophys. Res.-Atmos.*, 112, 19,
472 10.1029/2006jd007488, 2007.
- 473 Ricchiazzi, P., Yang, S. R., Gautier, C., and Sowle, D.: SBDART: A research and teaching software tool for plane-parallel radiative
474 transfer in the Earth's atmosphere, *Bulletin of the American Meteorological Society*, 79, 2101-2114, 10.1175/1520-



- 475 0477(1998)079<2101: Sarats>2.0.Co;2, 1998.
- 476 Schwarz, J. P., Gao, R. S., Fahey, D. W., Thomson, D. S., Watts, L. A., Wilson, J. C., Reeves, J. M., Darbeheshti, M., Baumgardner,
477 D. G., Kok, G. L., Chung, S. H., Schulz, M., Hendricks, J., Lauer, A., Karcher, B., Slowik, J. G., Rosenlof, K. H., Thompson, T. L.,
478 Langford, A. O., Loewenstein, M., and Aikin, K. C.: Single-particle measurements of midlatitude black carbon and light-scattering
479 aerosols from the boundary layer to the lower stratosphere, *J. Geophys. Res.-Atmos.*, 111, 15, 10.1029/2006jd007076, 2006.
- 480 Schwarz, J. P., Spackman, J. R., Fahey, D. W., Gao, R. S., Lohmann, U., Stier, P., Watts, L. A., Thomson, D. S., Lack, D. A., Pfister,
481 L., Mahoney, M. J., Baumgardner, D., Wilson, J. C., and Reeves, J. M.: Coatings and their enhancement of black carbon light
482 absorption in the tropical atmosphere, *J. Geophys. Res.-Atmos.*, 113, 10, 10.1029/2007jd009042, 2008.
- 483 Szopa, S., Naik, V., Adhikary, B., Artaxo, P., Bernsten, T., Collins, W. D., Fuzzi, S., Gallardo, L., Kiendler Scharr, A., Klimont, Z.,
484 Liao, H., Unger, N., and Zanis, P.: Short-Lived Climate Forcers. In *Climate Change 2021: The Physical Science Basis. Contribution*
485 *of Working Group I to the Sixth Assessment Report of the Intergovernmental Panel on Climate Change*, edited by: Masson-Delmotte,
486 V., Zhai, P., Pirani, A., Connors, S. L., Péan, C., Berger, S., Caud, N., Chen, Y., Goldfarb, L., Gomis, M. I., Huang, M., Leitzell, K.,
487 Lonnoy, E., Matthews, J. B. R., Maycock, T. K., Waterfield, T., Yelekçi, O., Yu, R., and Zhou, B., Cambridge University Press. In
488 Press., 2021.
- 489 Tan, W. S., Zhao, G., Yu, Y. L., Li, C. C., Li, J., Kang, L., Zhu, T., and Zhao, C. S.: Method to retrieve cloud condensation nuclei
490 number concentrations using lidar measurements, *Atmospheric Measurement Techniques*, 12, 3825-3839, 10.5194/amt-12-3825-
491 2019, 2019.
- 492 Tavakoli, F., and Olfert, J. S.: An Instrument for the Classification of Aerosols by Particle Relaxation Time: Theoretical Models of
493 the Aerodynamic Aerosol Classifier, *Aerosol Science and Technology*, 47, 916-926, 10.1080/02786826.2013.802761, 2013.
- 494 Wang, H. L., An, J. L., Zhu, B., Shen, L. J., Duan, Q., and Shi, Y. Z.: Characteristics of Carbonaceous Aerosol in a Typical Industrial
495 City-Nanjing in Yangtze River Delta, China: Size Distributions, Seasonal Variations, and Sources, *Atmosphere*, 8, 14,
496 10.3390/atmos8040073, 2017.
- 497 Wang, J. D., Wang, S. X., Wang, J. P., Hua, Y., Liu, C., Cai, J., Xu, Q. C., Xu, X. T., Jiang, S. Y., Zheng, G. J., Jiang, J. K., Cai, R.
498 L., Zhou, W., Chen, G. Z., Jin, Y. Z., Zhang, Q., and Hao, J. M.: Significant Contribution of Coarse Black Carbon Particles to Light
499 Absorption in North China Plain, *Environ. Sci. Technol. Lett.*, 9, 134-139, 10.1021/acs.estlett.1c00953, 2022.
- 500 Wex, H., Neususs, C., Wendisch, M., Stratmann, F., Koziar, C., Keil, A., Wiedensohler, A., and Ebert, M.: Particle scattering,
501 backscattering, and absorption coefficients: An in situ closure and sensitivity study, *J. Geophys. Res.-Atmos.*, 107, 18,
502 10.1029/2000jd000234, 2002.
- 503 Yu, H., Wu, C., Wu, D., and Yu, J. Z.: Size distributions of elemental carbon and its contribution to light extinction in urban and
504 rural locations in the pearl river delta region, China, *Atmospheric Chemistry and Physics*, 10, 5107-5119, 10.5194/acp-10-5107-
505 2010, 2010.
- 506 Zhang, R. Y., Khalizov, A. F., Pagels, J., Zhang, D., Xue, H. X., and McMurry, P. H.: Variability in morphology, hygroscopicity, and



507 optical properties of soot aerosols during atmospheric processing, Proceedings of the National Academy of Sciences of the United
508 States of America, 105, 10291-10296, 10.1073/pnas.0804860105, 2008.

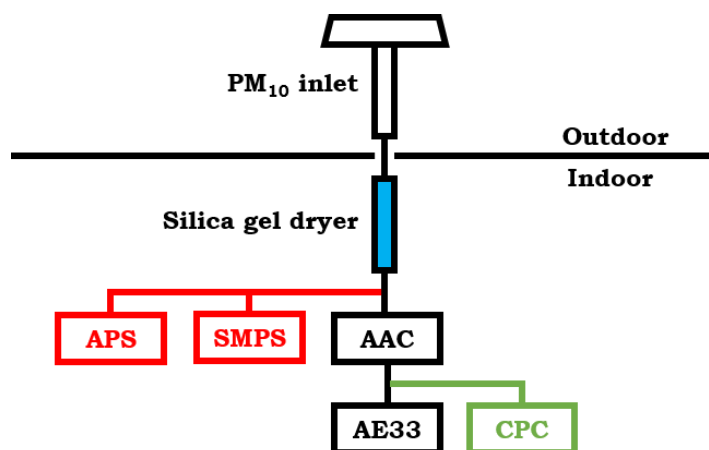
509 Zhao, G., Zhao, C. S., Kuang, Y., Bian, Y. X., Tao, J. C., Shen, C. Y., and Yu, Y. L.: Calculating the aerosol asymmetry factor based
510 on measurements from the humidified nephelometer system, Atmospheric Chemistry and Physics, 18, 9049-9060, 10.5194/acp-18-
511 9049-2018, 2018.

512 Zhao, G., Tao, J. C., Kuang, Y., Shen, C. Y., Yu, Y. L., and Zhao, C. S.: Role of black carbon mass size distribution in the direct
513 aerosol radiative forcing, Atmospheric Chemistry and Physics, 19, 13175-13188, 10.5194/acp-19-13175-2019, 2019.

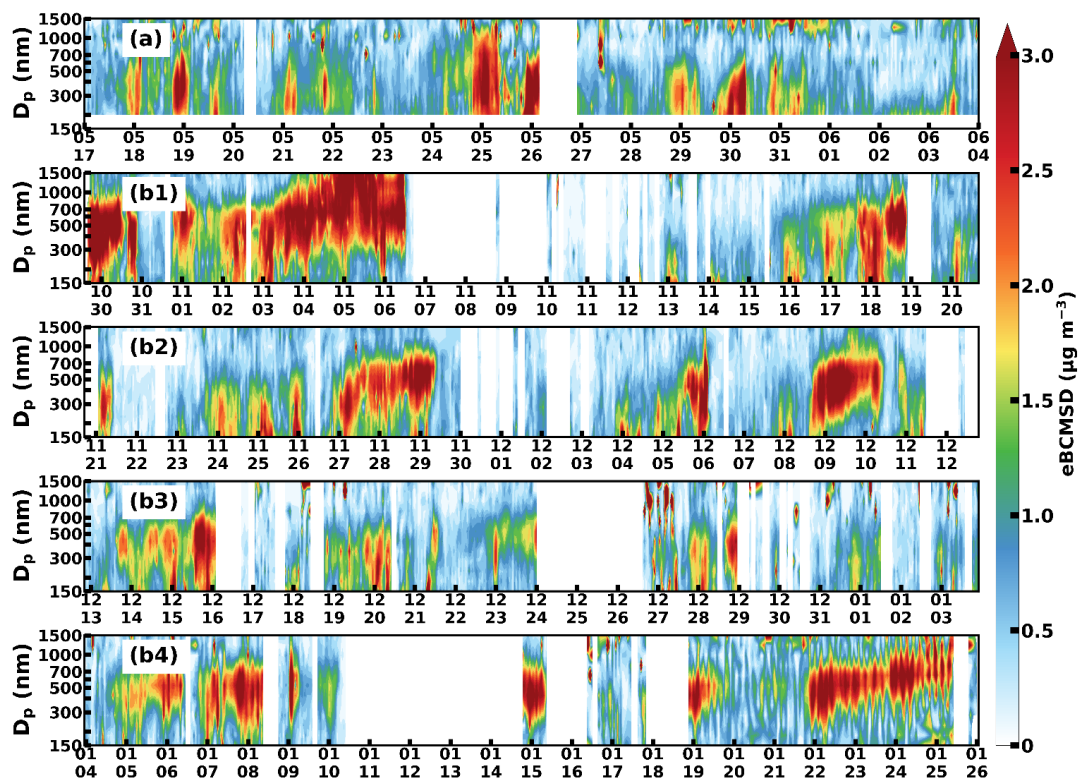
514 Zhao, W., Zhao, G., Li, Y., Guo, S., Ma, N., Tang, L., Zhang, Z., and Zhao, C.: New method to determine black carbon mass size
515 distribution, Atmos. Meas. Tech., 15, 6807-6817, 10.5194/amt-15-6807-2022, 2022.

516 Zhao, W. L., Tan, W. S., Zhao, G., Shen, C. Y., Yu, Y. L., and Zhao, C. S.: Determination of equivalent black carbon mass
517 concentration from aerosol light absorption using variable mass absorption cross section, Atmospheric Measurement Techniques,
518 14, 1319-1331, 10.5194/amt-14-1319-2021, 2021.

519



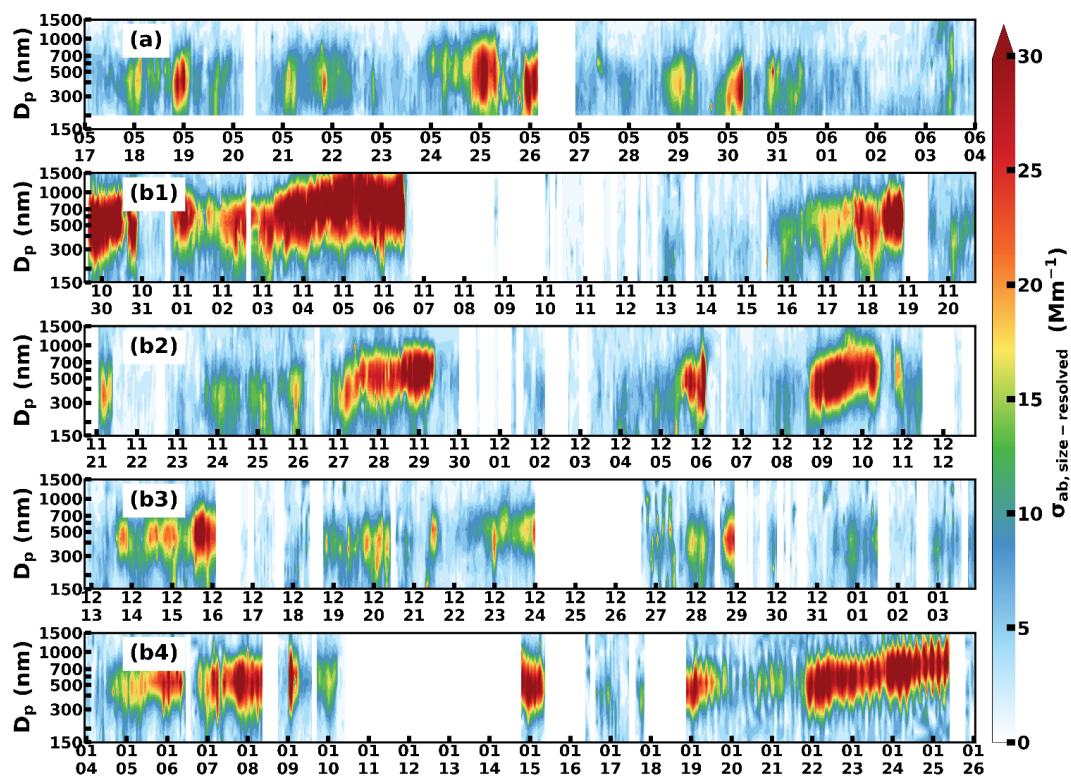
520
521 **Figure 1: Instrumental setup used in this study. Instruments used to measure $N_{\text{size-resolved}}$ was colored with red (green) for**
522 **Changzhou (Beijing).**
523



524

525 Figure 2: Time series of eBCMSD measured in (a) Changzhou from May 17th 2021 to June 3rd 2021 and (b1 – b4)

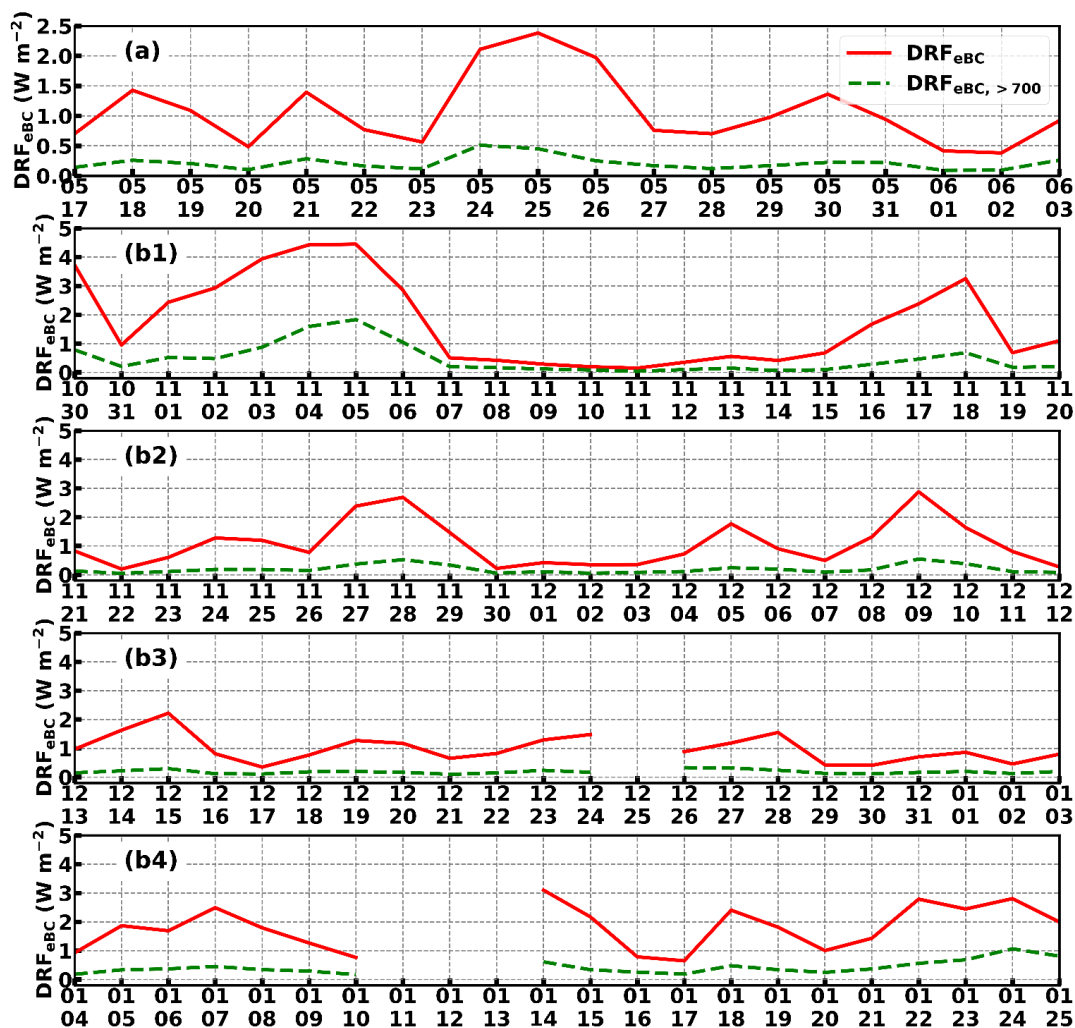
526 Beijing October 29th 2021 to January 25th 2022. (b1) to (b4) corresponded to different time ranges.



527

528 Figure 3: Same as Fig. 2, except for $\sigma_{ab, \text{size-resolved}}$.

529

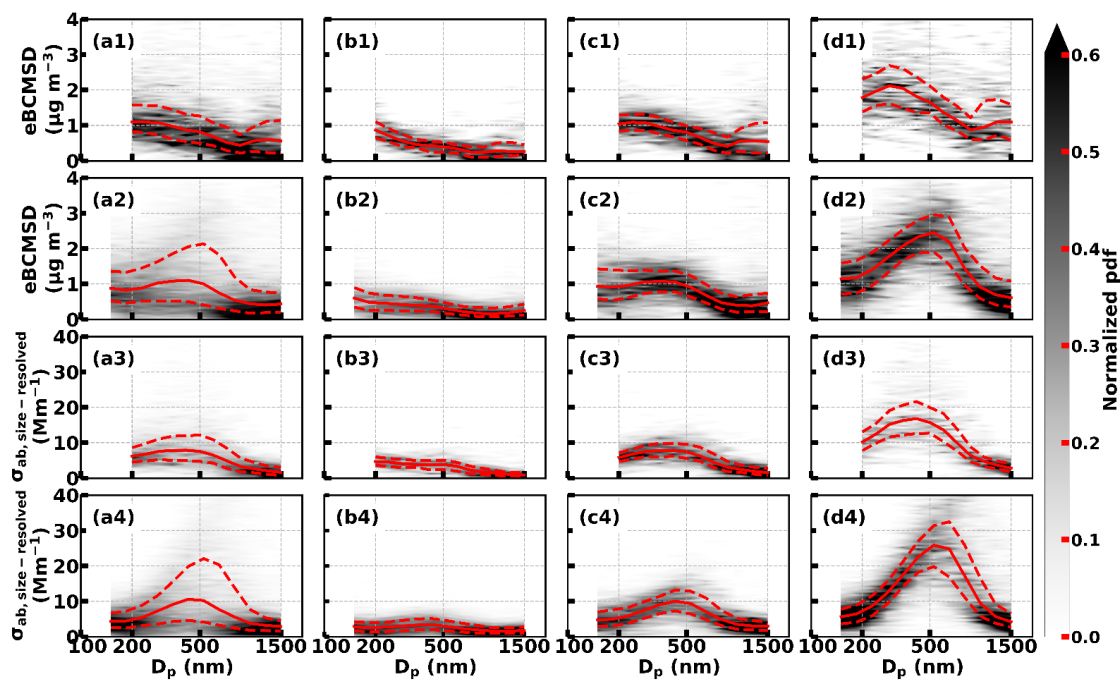


530

531

Figure 4: Same as Fig. 2, except for DRF_{eBC} (red solid line) and $DRF_{eBC, >700}$ (green dashed line).

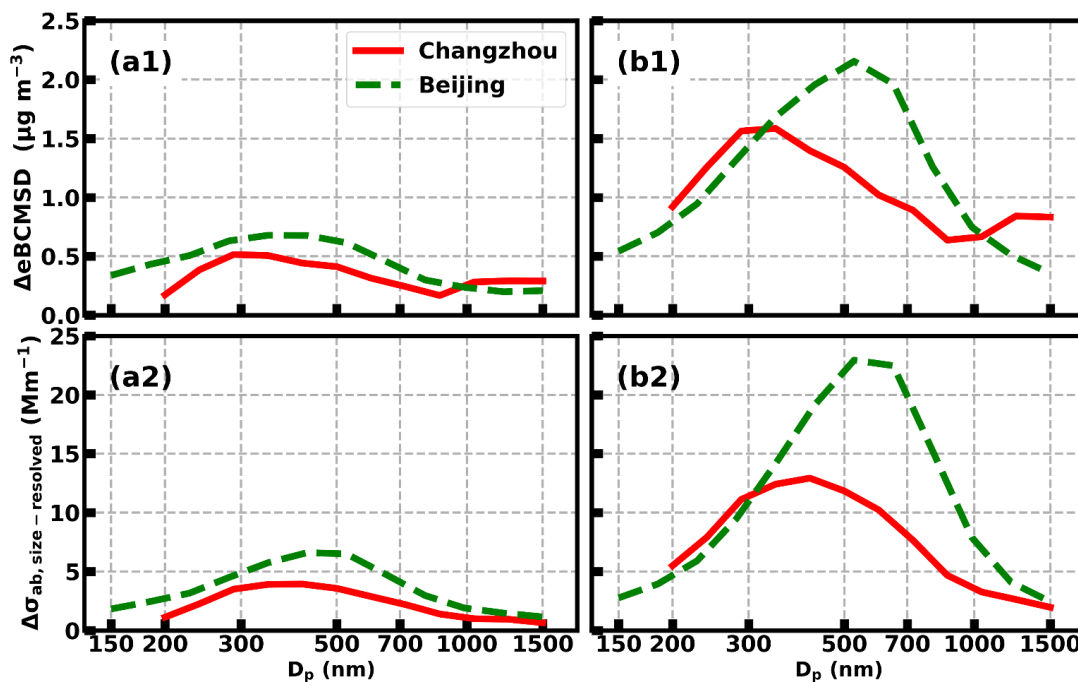
532



533

534 **Figure 5: Normalized pdf of eBCMSD measured in (a1 – d1) Changzhou and (a2 – d2) Beijing as well as $\sigma_{ab,size-resolved}$**
535 **measured in (a3 – d3) Changzhou and (a4 – d4) Beijing. (a1 – a4), (b1 – b4), (c1 – c4) and (d1 – d4) were statistics over**
536 **the whole campaign, clean period, transitional period and polluted period. Red solid line and red dashed lines were**
537 **median and lower as well as upper quartiles.**

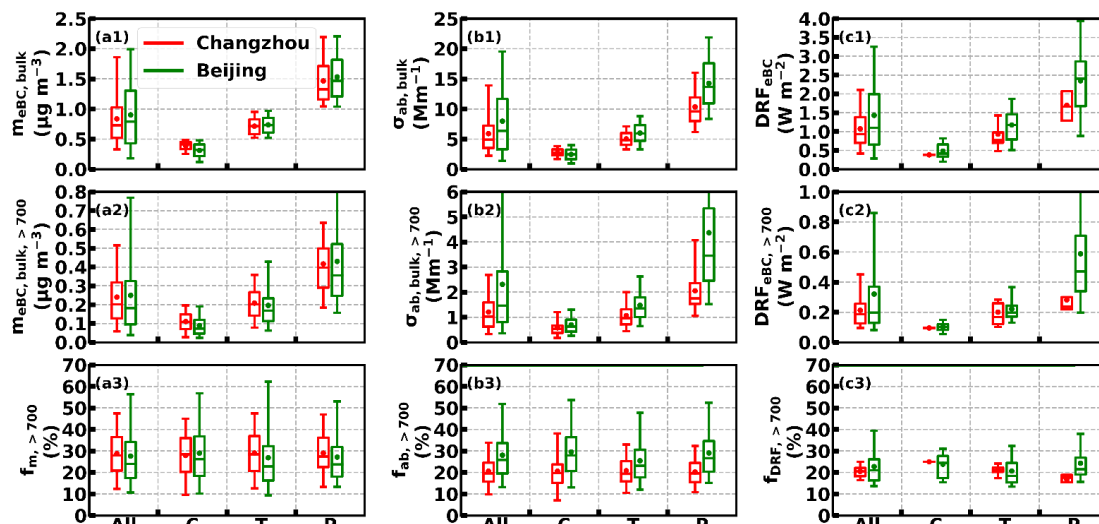
538



539

540 Figure 6: Increase of median eBCMSD in (a1) transitional and (b1) polluted period relative to clean period as well as
 541 increase of median $\sigma_{ab,size-resolved}$ in (a2) transitional and (b2) polluted period relative to clean period. Red solid (green
 542 dashed) line stood for Changzhou (Beijing).

543

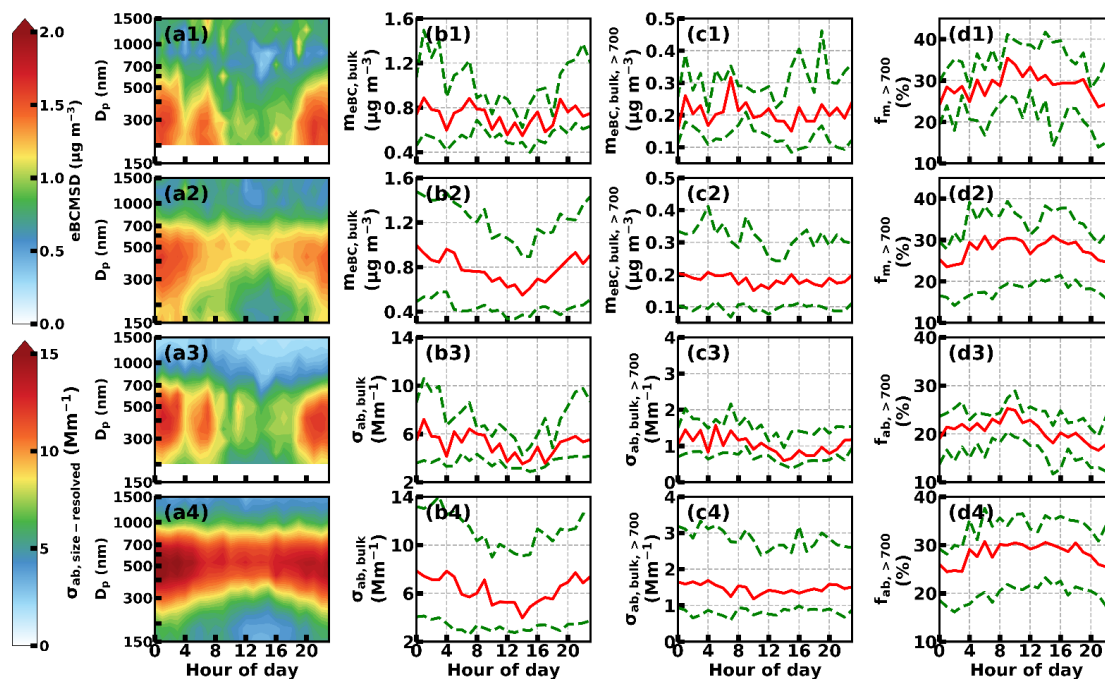


544

545 Figure 7: Box plots of (a1) $m_{eBC,bulk}$, (a2) $m_{eBC,bulk,>700}$, (a3) $f_{m,>700}$, (b1) $\sigma_{ab,bulk}$, (b2) $\sigma_{ab,bulk,>700}$, (b3) $f_{ab,>700}$, (c1) DRF_{eBC} ,
 546 (c2) $DRF_{eBC,>700}$ and (c3) $f_{DRF,>700}$ over the whole campaign (All), clean (C), transitional (T) as well as polluted (P) period,
 547 respectively. The box extended from the first quartile to the third quartile with a line at the median. The whiskers



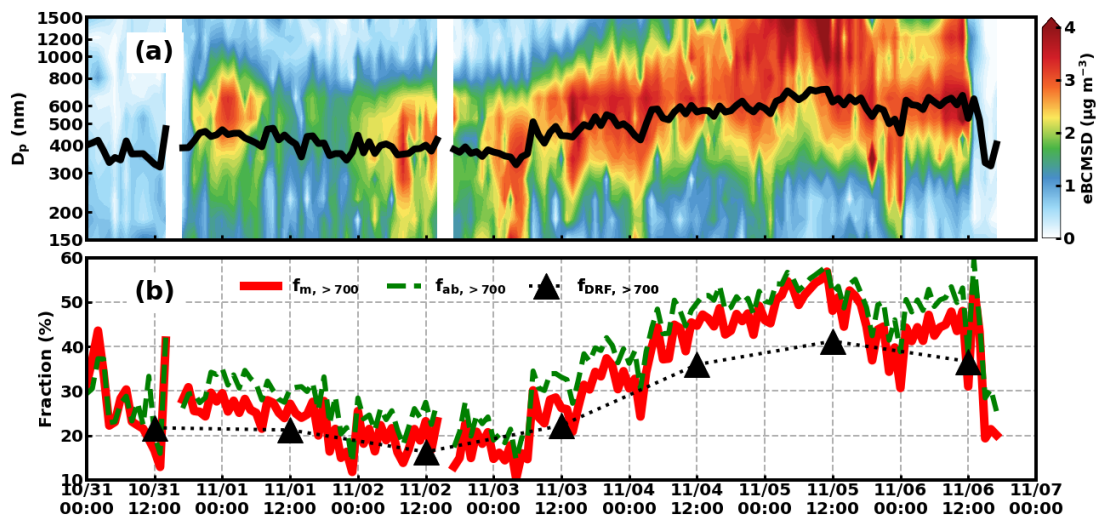
548 marked 5 % and 95 % percentile. The circle inside the box was the mean value. Statistics from Changzhou (Beijing)
 549 were colored red (green). The 95 percentile of $m_{\text{eBC,bulk},>700}$ under polluted period for Beijing (a2) was $1.00 \mu\text{g m}^{-3}$. The
 550 95 percentile of $\sigma_{\text{ab,bulk},>700}$ and that under polluted period for Beijing (b2) was 7.80 and 10.30 Mm^{-1} , respectively. The
 551 95 percentile of $\text{DRF}_{\text{eBC},>700}$ under polluted period for Beijing (c2) was 1.41 W m^{-2} .
 552



553

554 **Figure 8:** Diurnal variation of (a1) eBCMSD, (b1) $m_{\text{eBC,bulk}}$, (c1) $m_{\text{eBC,bulk},>700}$, (d1) $f_{m,>700}$ in Changzhou; (a2) eBCMSD,
 555 (b2) $m_{\text{eBC,bulk}}$, (c2) $m_{\text{eBC,bulk},>700}$, (d2) $f_{m,>700}$ in Beijing; (a3) $\sigma_{\text{ab,size-resolved}}$, (b3) $\sigma_{\text{ab,bulk}}$, (c3) $\sigma_{\text{ab,bulk},>700}$, (d3) $f_{\text{ab},>700}$ in
 556 Changzhou and (a4) $\sigma_{\text{ab,size-resolved}}$, (b4) $\sigma_{\text{ab,bulk}}$, (c4) $\sigma_{\text{ab,bulk},>700}$, (d4) $f_{\text{ab},>700}$ in Beijing. Red solid line and green dashed
 557 lines were median and lower as well as upper quartiles.

558



559

560 Figure 9: (a) eBCMSD from October 31st 2021 to November 6th 2021 in Beijing and (b) the corresponding $f_{m,>700}$ (red
561 solid line), $f_{ab,>700}$ (green dashed line) as well as $f_{DRF,>700}$ (black dotted line with triangle marker). The black solid line
562 was \bar{D}_p .